NANOSYSTEMS: PHYSICS, CHEMISTRY, MATHEMATICS, 2016, 7 (4), P. 583–591

Optical properties of sodium niobate thin films

V. Lingwal[1], A. S. Kandari[2], N. S. Panwar[2]

[1]Pt. L.M.S. Govt. PG College Rishikesh, Uttarakhand, 249 201, India

[2]USIC, HNB Garhwal University, Srinagar (Garhwal), Uttarakhand, 246 174, India

lingwalv@yahoo.co.in, kandarialok@gmail.com, nspusic@gmail.com

PACS 77.55.fj, 78.20.Ci **DOI 10.17586/2220-8054-2016-7-4-583-591**

$NaNbO_3$ thin films were deposited under different conditions by rf magnetron sputtering of ceramic target. Spectral transmission of the deposited films was measured in the UV-Visible-near IR range. Films deposited at 300 °C showed more absorption, and films annealed at 300 °C showed less absorption than those deposited at room temperature (RT), which was found to be consistent with their X-ray diffraction (XRD) patterns. From the observed transmission spectra, refractive index, optical band gap, absorption coefficient, extinction coefficient and film thickness were calculated for the deposited films. Refractive index at 550 nm wavelength was found to be 2.11, 2.01 and 2.34 for the films deposited at RT, 300 °C and annealed at 300 °C, respectively. The refractive index was found to be almost constant with respect to frequency for the films annealed at 300 °C. Optical band gap was found 3.82, 3.7 and 3.81 eV for the films deposited at RT, 300 °C, and annealed at 300 °C, respectively. Film thickness was shown to decrease with annealing. Absorption and extinction coefficients decreased with increasing wavelength, in all the samples. Band gaps associated with different interactions have been calculated for the deposited films. Phonon assisted indirect forbidden transition was most favorable in the deposited films.

Keywords: Ferroelectrics, antiferroelectrics, thin films, sputtering, transmission.

Received: 27 January 2016

Revised: 21 June 2016

1. Introduction

The physical properties of thin film material depend on its thickness, surface to volume ratio, microstructure and microchemistry; which strongly depend on its growth process. The most conspicuous phenomena associated with thin films are optical ones. The studies on electric properties as well as the emission of electrons from thin films have made extraordinarily rapid advances in recent years, due to their wide tailor-made applications.

Dielectric materials employed in optical coatings include fluorides (e.g., MgF_2, CeF_3), oxides (e.g., Al_2O_3, TiO_2, SiO_2, Ta_2O_5), sulfides (e.g., ZnS, CdS), assorted compounds (e.g., ZnSe, ZnTe), etc. An essential common feature of dielectric optical materials is their low absorption coefficients ($\alpha < 10^3$/cm) in some relevant portion of the spectrum, where they are essentially transparent. Ferroelectric materials, such as $LiNbO_3$, $KNbO_3$, K(Ta, Nb)O_3, $PbTiO_3$ based materials, etc., are useful in optical applications, e,g., in infrared detectors, optical waveguide devices, optical memories and displays, spatial light modulators, frequency doublers for diode lasers, etc. [1–11]. Application of ferroelectric films in these devices hinges on successful integration of ferroelectric films into semiconductors or other useful substrates.

Nonmetallic materials may be opaque or transparent to visible light, and if transparent, they often appear colored. In principle, light radiation is absorbed in this group of materials by three basic mechanisms; viz., electronic polarization, electronic transitions across the band gap and electronic excitations to impurity or defect levels, which also influence their transmission characteristics. Absorption by electronic polarization is important only at light frequencies in the vicinity of the relaxation frequency of the constituent atoms. The other two mechanisms involve electron transitions, which depend on the electronic energy band structure of the materials; one of these absorption mechanisms involves the absorption as a consequence of electron excitations across the band-gap; the other is related to electron excitations to impurity or defect levels that lie within the band gap. Absorption of a photon may promote or excite an electron, across the band gap, from the nearly filled valence band to an empty state within the conduction band, thus creating a free electron in the conduction band and a hole in the valence band. The excitation energy E is related to the absorbed photon frequency (ν); i.e., $E = h\nu$. These excitations with the accompanying absorption can take place only if the photon's energy is greater than that of the band gap E_g, i.e., if $h\nu > E_g$. At the minimum wavelength for visible light, $E = 3.1$ eV, means no visible light is absorbed by nonmetallic materials having band gap energy (Eg) greater than about 3.1 eV; these materials, if of high purity, will appear transparent and colorless. Optical measurements constitute the most important means of determining the inter-band structure of the materials. Photon induced inter-band electronic transitions can occur between different bands. Also optical measurements can be used to study lattice vibrations.

In the present study, $NaNbO_3$ films were deposited on the quartz substrate using the rf magnetron sputtering method. Films were deposited at room temperature and at varying substrate temperatures. The room temperature deposited films were annealed at different temperatures. Optical parameters were measured for $NaNbO_3$ films deposited at room temperature, at 300 °C, and post deposition annealed at 300 °C. Deposited films were characterized using XRD method.

2. Preparation

Thin films of $NaNbO_3$ were deposited by the rf magnetron sputtering of bulk $NaNbO_3$ pellet targets. Films were deposited on to clean Quartz (Qz) and monocrystalline silicon surfaces. Ceramic pellets of $NaNbO_3$ of 36 mm diameter and 2.5 mm thickness were used as sputtering targets. The targets were prepared by the conventional solid-state reaction method. The pumping system used was a combination of 300 l/sec diffusion pump and a 200 l/min rotary pump. The system gives an ultimate vacuum of 3×10^{-5} mbar. The pressure was monitored using a Pirani and a Penning gauge combination. The vacuum chamber was a 300 mm diameter stainless steel cylinder. The target disk was mechanically clamped to a water-cooled assembly with magnetic arrangement. The system was arranged in sputter down configuration with a substrate-target distance of 30 mm. Separate feed-troughs were fitted for heater connections, and for the thermocouple that is used in contact with the substrate to estimate its temperature. Argon (99.999 %) was used as sputtering gas. An rf system from CVC Scientific Products Ltd, Wakingham, England, was used for sputtering. Films were deposited at a working pressure of 1×10^{-3} mbar, for 30 minutes, at different substrate temperatures. All the films were deposited at a forward power of 30 W, whereas reverse power was zero. The cleanliness of the substrate's surface exerts a decisive influence on film growth and adhesion. A thoroughly cleaned substrate is a prerequisite for the preparation of films with reproducible properties. Quartz substrates were rinsed with a laboratory detergent and then rinsed with distilled water and lastly wiped with soft dry cloth with little trace of acetone. The temperature of the substrate was monitored using a cromel-alumel thermocouple. The deposited films were left in the chamber for 2 hrs and then removed for experimental investigations. The films deposited at room temperature were annealed post-deposition, in a furnace at different temperatures, in the presence of ambient oxygen.

3. Characterization

3.1. X-ray diffraction patterns

The structures of the deposited $NaNbO_3$ films, at room temperature (RT) and at substrate temperature 225, 270, 300 and 375 °C, were studied by x-ray diffraction with the help of Philips Analytical X-ray Diffractometer (PW 3710), using $CuK\alpha_1$ radiation of wavelength 1.54056 Å. Peak indexing was done by using the Joint Committee on Powder Diffraction Standards (JCPDS) data cards. The XRD patterns obtained are shown in Fig. 1. The RT deposited films exhibited crystalline structure with different orientations. However, it has been reported earlier that oxide films deposited at RT, generally, show amorphous nature and crystalline structure is set at higher temperatures [12–15].

The experimental investigations have shown that the properties of oxides depend on its growth process and post annealing process [15]. To study the effect of annealing, films deposited at RT were annealed at 400, 500 and 600 °C. The XRD patterns of annealed films are depicted in Fig. 2.

From the XRD patterns of $NaNbO_3$ films deposited at different substrate temperatures (at 225, 270, 300 and 375 °C) (Fig. 1), it has been observed that films deposited at 225 and 270 °C show crystalline structure with single face orientation while films deposited at substrate temperatures of 300 and 375 °C showed amorphous nature.

From the XRD patterns of the annealed films (Fig. 2), it has been observed that annealing up to 500 °C changes the orientation of the deposited films, and annealing at higher temperature (600 °C) shows amorphous films. The observed amorphous nature of the films annealed at higher temperatures ($\geq$ 600 °C) may be due to a deficiency of volatile sodium ions. The films deposited at RT were oriented in (101) and (221) directions. Films deposited at substrate temperatures of 225 and 270 °C and the films annealed at 400 and 500 °C showed orientation towards the (002) plane. This orientation is due to the coalescing islands, which proceed until the film reaches continuity.

3.2. Transmission spectra

The spectral transmissions (at 6 ° angle of incidence) of the $NaNbO_3$ films were measured using a UV-visible-near infrared double beam spectrophotometer (Hitachi, model 330). The observed transmission spectra of the $NaNbO_3$ films deposited at different conditions are shown in Figs. 3 – 5. It has been observed that the films deposited at 300 °C substrate temperature show more absorption while those films annealed at 300 °C shows less

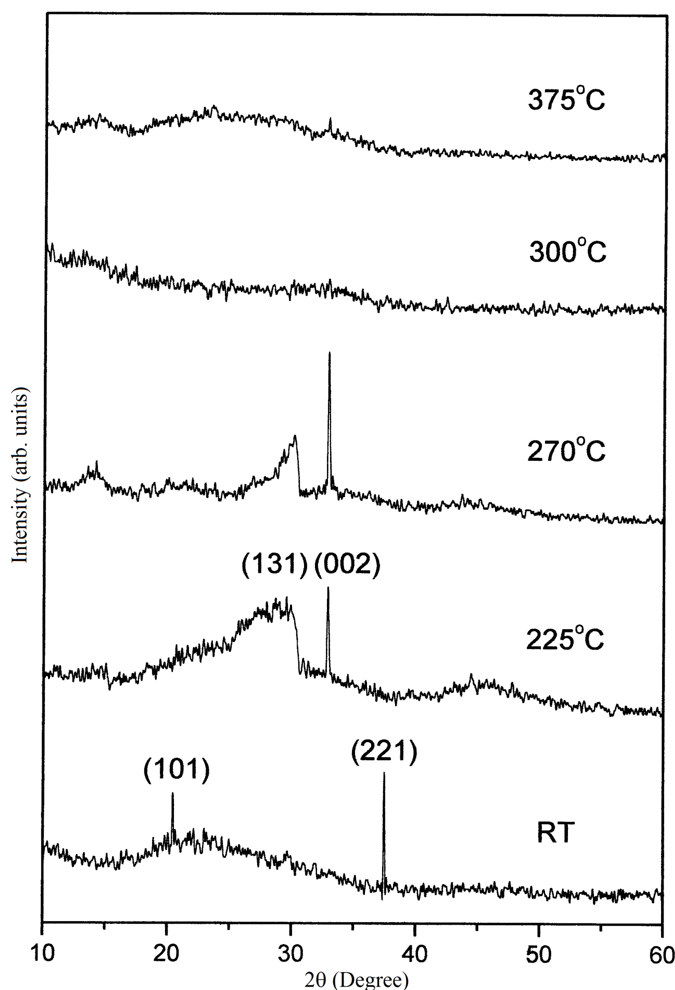

FIG. 1. X-ray diffraction patterns of $NaNbO_3$ films, deposited at different substrate temperatures

absorption than the films deposited at RT. The observed high absorption of the films also suggests an amorphous nature for the deposited films at higher substrate temperature, as has been observed in the XRD study. The lower absorption of the annealed films, at 300 °C, suggests a reorientation of the film crystallites in single face and also to the decrease in oxygen vacancies in the deposited films when annealed in the presence of ambient oxygen, as has been observed from the XRD patterns. The increase in absorption in the films, deposited at 300 °C, may be due to the higher oxygen deficiency and some amount of sodium deficiency, so the deposited films may not be in stoichiometric composition [16]. These deficiencies, in the films, may also be caused by the preferential sputtering, which removes atoms from the film leaving the deposited film sub-stoichiometric [17].

The preferential sputtering in oxide thin films can be explained on the basis of Winter and Sigmund model [16], according to which, the energy transfer coefficient in a head on collision process between an ion of mass m and a target of mass M is given by $E_T = 4mM/(m + M)^2$. Applying this equation to the collision of oxygen with oxygen and niobium atoms of the growing film, with oxygen, yields value of E_T as 1.0 for oxygen-oxygen and 0.5 for oxygen-niobium collision. This means that only 50 % of the energy is transferred in the case of oxygen-niobium collisions. Hence, more energy is delivered to the oxygen atoms than to the niobium atoms, leading to higher re-sputtering of oxygen atoms from the film. Compounds made up of elements with smaller difference in masses have fewer tendencies to be sputtered out from the film. The sub-stoichiometry causes degradation in the refractive index of the film.

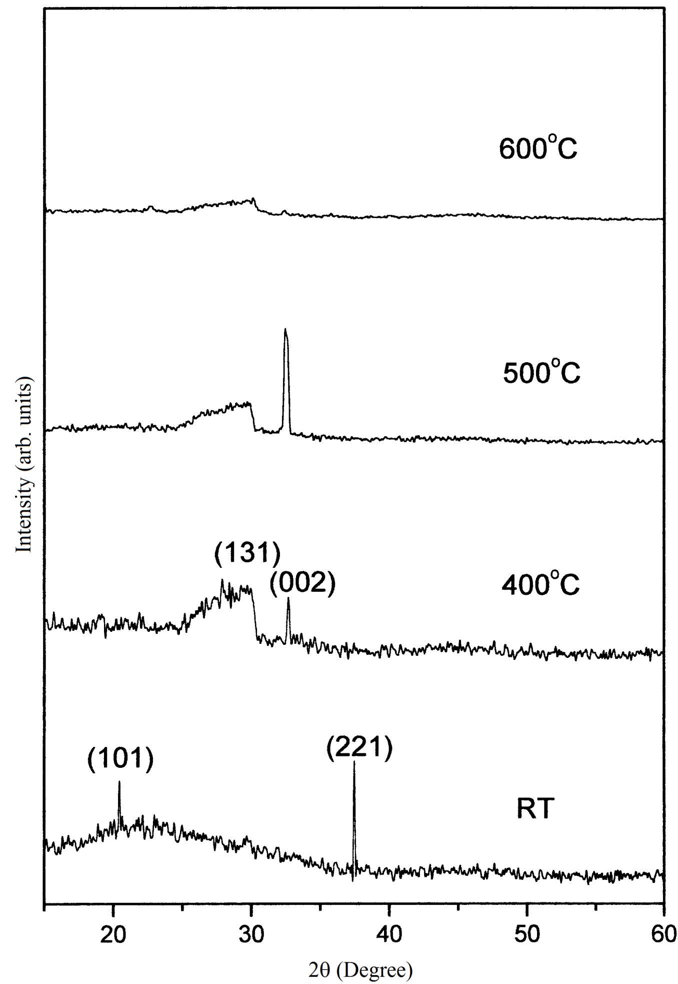

FIG. 2. X-ray diffraction patterns of $NaNbO_3$ films, deposited at room temperature (RT) and annealed at different temperatures

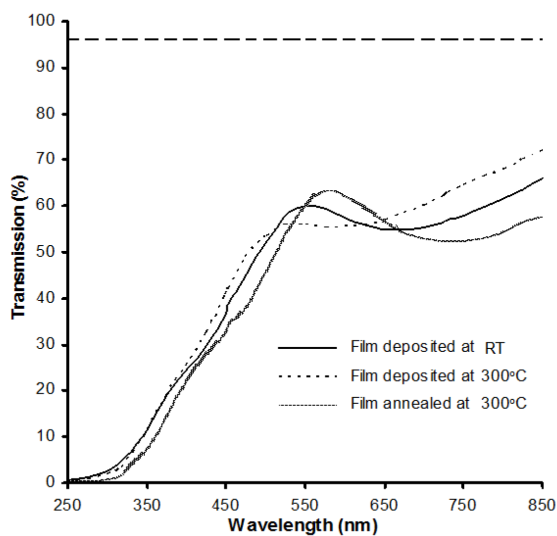

FIG. 3. Transmission spectra of $NaNbO_3$ films prepared at different conditions

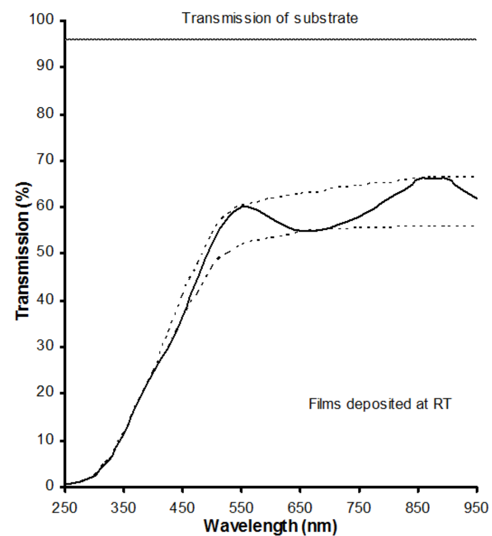

FIG. 4. Envelope of the transmission spectra of the $NaNbO_3$ films, deposited at RT

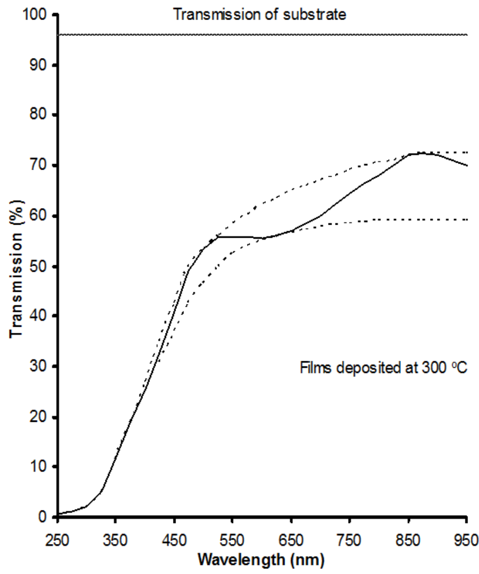

FIG. 5. Envelope of the transmission spectra of the $NaNbO_3$ films, deposited at 300 °C

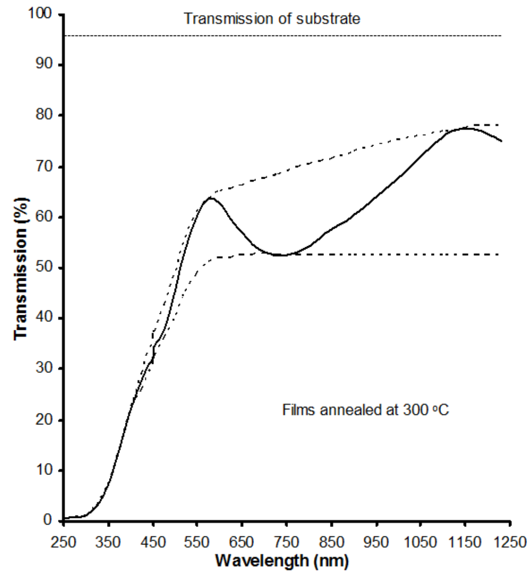

FIG. 6. Envelope of the transmission spectra of the $NaNbO_3$ films, annealed at 300 °C

4. Optical properties

Optical constants, such as, refractive index (n), optical band gap (E_g), absorption coefficient (α), extinction coefficient (k), and thickness of the films have been calculated, for $NaNbO_3$ films deposited on quartz (Qz) substrate ($n = 1.55$, transmittance $= 0.96$), using Swanepoel's envelope technique [18].

It is clear from Figs. 4 – 6 that the transmission in the film samples, deposited at the substrate temperature 300 °C, is lower than that the samples deposited at RT. It shows high absorption in the samples deposited at 300 °C substrate temperature, and thereby showing amorphous nature, which is in conformity with the results obtained from XRD patterns, Fig. 1. The film absorption has been reported to increase with high-level substrate temperature [12]. The absorption is low in the samples annealed at 300 °C, indicating good quality of $NaNbO_3$ films, Fig. 5. The low absorption in the films deposited at RT in comparison to that in the films annealed at 300 °C (as confirmed by XRD patterns, Fig. 2) may be attributed to the variation in the rate of re-crystallization, in these samples. Meanwhile, the peak transmission of all the films deposited in the present study is very much lower than that of the quartz substrate used, indicating very high absorption in these films. No many maxima and minima were observed in the transmission spectra of the present samples, which may be due to non-uniformity in the film thickness.

4.1. Refractive index (n)

According to Swanepoel's envelope technique [18], the refractive index (n), at wavelength λ, is given by

$$n(\lambda) = \left(N + \left(N^2 - n_s^2\right)^{1/2}\right)^{1/2},$$

where n_s is the refractive index of the substrate, at wavelength λ, and

$$N = \frac{2n_s\left[T_M(\lambda) - T_m(\lambda)\right]}{T_M(\lambda)\, T_m(\lambda)} + \frac{n_s^2 + 1}{2},$$

where $T_M(\lambda)$ and $T_m(\lambda)$ are the transmission maxima and minima, respectively, corresponding to wavelength λ obtained from the envelope, as shown in Figs. 3 – 5.

Figure 6 shows the calculated values of n with λ for the films deposited at different conditions. At 550 nm wavelength, the refractive index (n) values for films deposited at RT and 300 °C were 2.11 and 2.01, respectively; and 2.34 for the samples annealed at 300 °C. The degradation of n in the samples deposited at higher substrate temperature is due to sub-stoichiometry in the films due to preferential sputtering in the deposited films. Fig. 7 shows that n decreases with increasing wavelength for the films deposited at RT, and at 300 °C; while n remains almost constant for the samples annealed at 300 °C. The low value of packing density in the samples may be one of the reasons for the decrease in n with increasing wavelength, in the samples deposited at RT and at 300 °C, since

these samples may be oxygen deficient. In the samples annealed at 300 °C, in the ambient oxygen atmosphere, the oxygen stoichiometry and hence the packing density improves, and n remains constant with varying wavelength. Value of n has been reported 2.21 for the single crystal of $NaNbO_3$ [19], at 550 nm.

4.2. Optical band gap

The excellent transmission of dielectric materials in the visible region of the spectrum is found to terminate at shorter wavelengths with the onset of the UV absorption edge. The critical radiation wavelength, λ_c, at which this occurs, is given by $\lambda_c(\mu m) = 1.24/E_g$ (eV). These values physically correspond to electronic transitions from the filled valence band levels, across the energy gap E_g, to the unfilled conduction band states. Multiple peaks near the UV absorption edge indicate the complexity of these processes. At long wavelengths, the high optical transmission is limited by absorption due to the vibration of lattice ions in resonance with the incident radiation. The frequency of maximum absorption is related to the force constant and masses of vibrating anions and cations. The optical band gaps for the films deposited at RT and at 300 °C has been calculated to be 3.82 and 3.7 eV, respectively; and for the films annealed, at 300 °C, this value was found to be 3.81 eV. The band gap for single $NaNbO_3$ crystal has been reported 3.4 eV [20].

4.3. Film thickness

The thickness (d) of the film is given by [18]:

$$d = \frac{\lambda_1 \lambda_2}{4\left(n_1 \lambda_2 - n_2 \lambda_1\right)},$$

where λ_1 and λ_2 are the wavelengths of two successive maxima and minima; n_1 and n_2 are the refractive indices at λ_1 and λ_2, respectively.

The calculated thicknesses of the films deposited at RT and 300 °C were obtained as 3455 and 5182 Å, respectively, while a value of 3132 Å was obtained for the films annealed at 300 °C after depositing at RT. The lowering of the thickness in the annealed samples may be explained on the basis of reduction of voids between islands during the process. The voids are filled up by coalescence process, recrystallization and reorientation of the film crystallites.

4.4. Absorption and inter-band transitions

Absorption coefficient (α) of the film is given by [18]:

$$\alpha = -\frac{\log(x)}{d},$$

where,

$$x = \frac{E_m - \left[E_m^2 - \left(n^2-1\right)^3\left(n^2 - n_s^4\right)\right]^{1/2}}{\left(n-1\right)^3\left(n - n_s^2\right)},$$

with

$$E_m = \frac{8n^2 n_s}{T_M} + \left(n^2-1\right)\left(n^2 - n_s^2\right),$$

n is the refractive index of the film; T_m is the maximum transmission of the film, and d is the film thickness.

The absorption coefficient (α) was found to decrease with increased wavelength for all the $NaNbO_3$ films, deposited under different conditions. The calculated value of α was determined to be 4.67×10^3 /cm for the samples deposited at RT, at 550 nm wavelength. In the region of strong absorption, the interference fringes disappear. Values for n in strong absorption region were estimated by extrapolating the values calculated in the other parts of the spectrum [18].

The extinction coefficient (k), at wavelength λ, is given by:

$$k = \frac{\alpha\lambda}{4\pi}.$$

Observations, shown in Fig. 8, indicate that k decreases with increasing wavelength, for all the $NaNbO_3$ film samples, prepared under different conditions. Also, Absorption coefficient may be expressed as a function of the incident photon energy, $h\nu$, as [21]:

$$\alpha(h\nu) = A\left(h\nu - E_g\right)^m, \tag{1}$$

where A and m are constants, and the value of m decides the nature of transition. These observations may be analyzed according to this relation. The value of E_g has been calculated at and beyond the absorption edge. The variations of the absorption coefficient with the incident photon energy have been plotted for the estimation

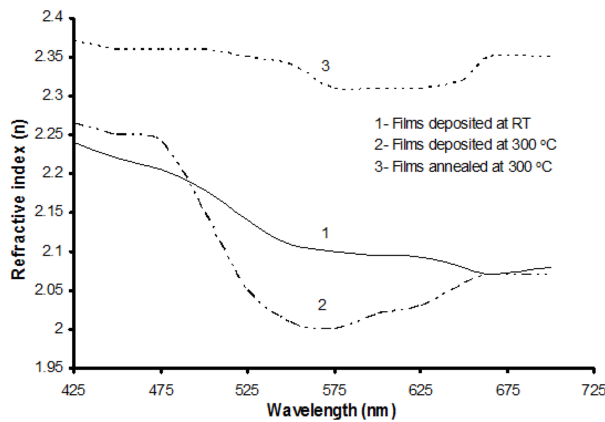

FIG. 7. Variation of refractive index with wavelength, of the $NaNbO_3$ films prepared at different conditions

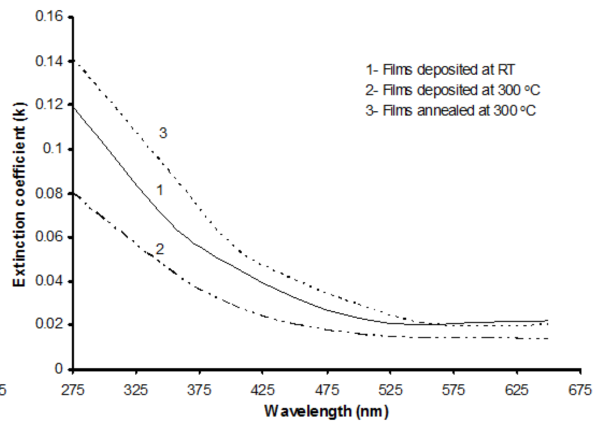

FIG. 8. Wavelength dependence of extinction coefficient of $NaNbO_3$ films, prepared at different conditions

of energy gap. The band gap was found to be composition dependent for dielectric films [22–25]. The radiation absorbed by a solid can be converted into elastic vibrations in it, and it may initiate photon-electron, photon-phonon and other interactions.

The photon-electron interaction leads to direct transition probability and this interaction satisfies Eq. (1) with $m = 1/2$. Figs. 9(a), 10(a) and 11(a) show α^2 *vs.* $h\nu$ curves, for the films deposited at RT, at 300 °C, and for the films annealed at 300 °C, respectively. Extrapolation of the straight portion of the curve, α^2 *vs.* $h\nu$, gives the direct allowed energy band gap of the film samples. The value for the direct allowed energy band gap was estimated from the intersection of the tangent, drawn near the absorption edge, in the α^2 *vs.* $h\nu$ plot (the straight line portion), with the energy axis. The direct allowed energy band gap values were obtained as 3.4 eV for the films deposited at room temperature and 300 °C, and 3.2 eV for the films annealed at 300 °C.

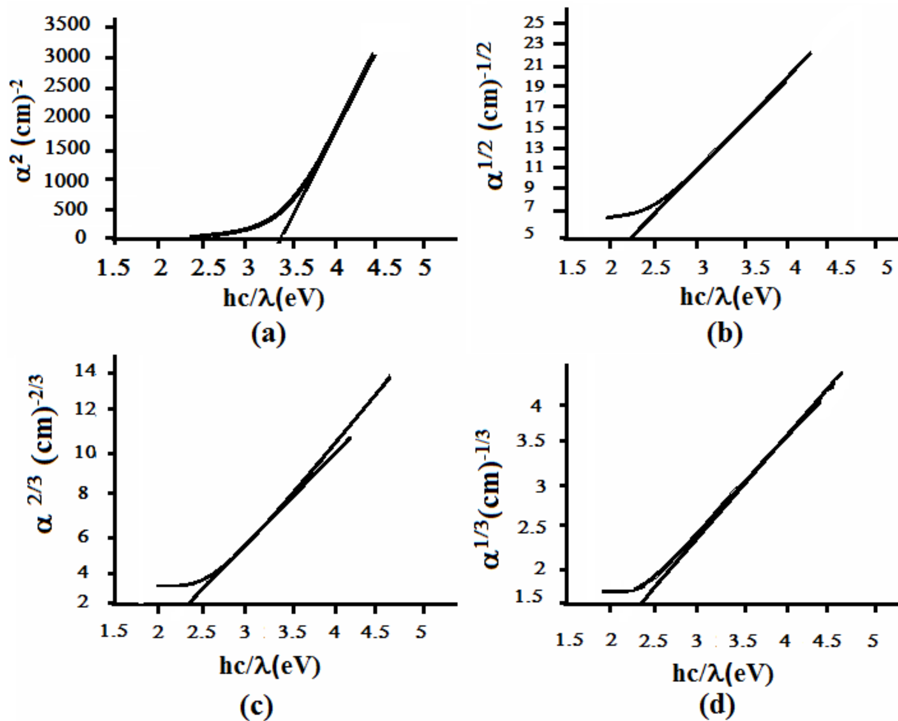

FIG. 9. α^m as a function of hc/λ, for different m values, in the samples deposited at RT

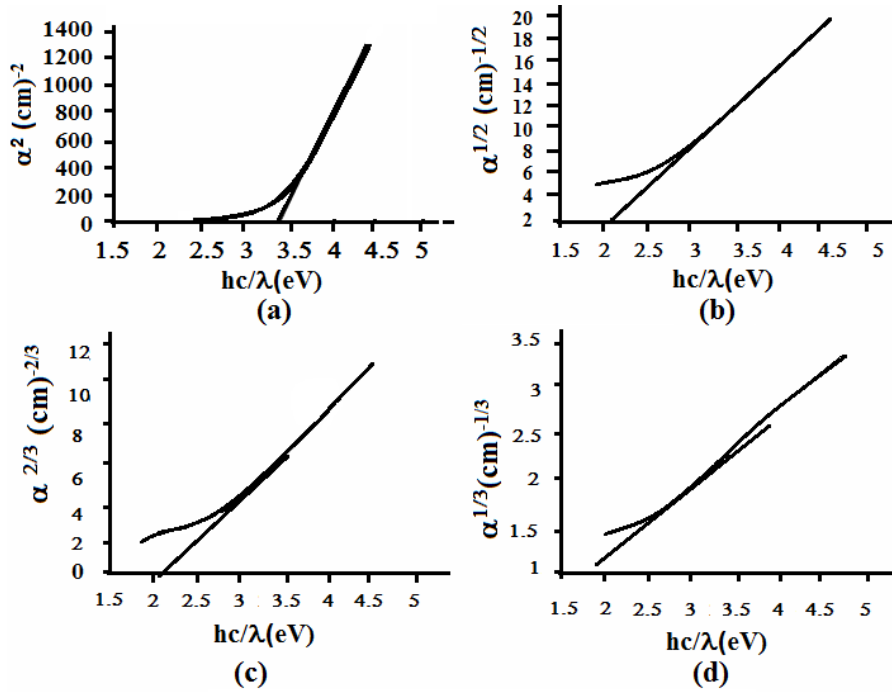

FIG. 10. α^m as a function of hc/λ, for different m values, in the samples deposited at 300 °C

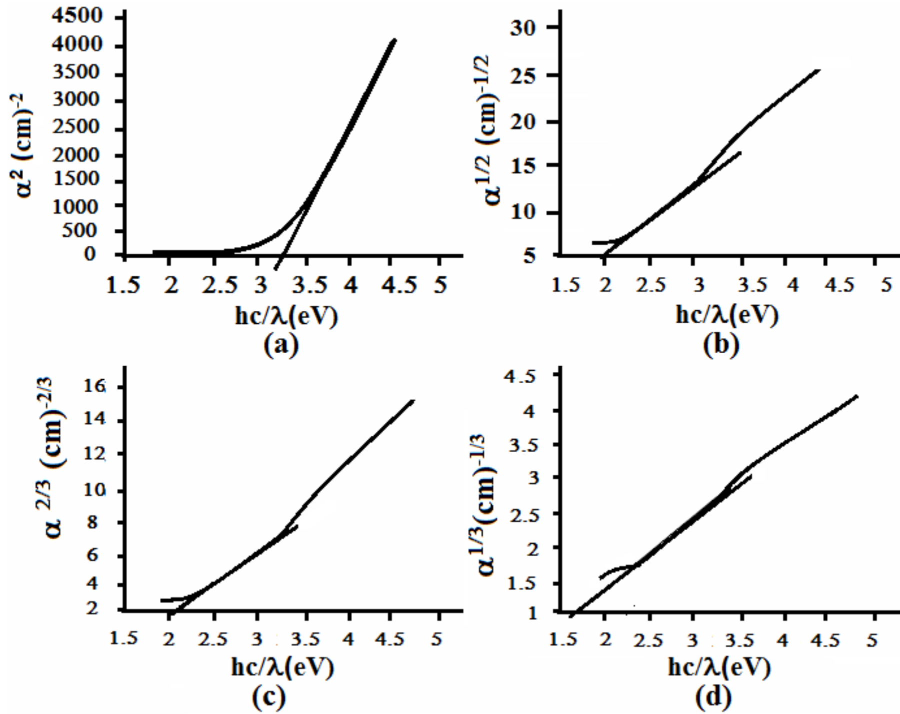

FIG. 11. α^m as a function of hc/λ, for different m values, in the samples annealed at 300 °C

The photon-phonon interaction leads to indirect allowed transition probability and is given by Eq. (1) with $m = 2$; and E_g is indirect allowed energy band gap. Figs. 9(b), 10(b) and 11(b) show the variation of $\alpha^{1/2}$ with $h\nu$. The indirect allowed energy band gap from the $\alpha^{1/2}$ *vs.* $h\nu$ plots is found to be 2.2, 2.09 and 2.0 eV; for the films deposited at RT, 300 °C, and for the films annealed at 300 °C, respectively.

In addition to the photon assisted electronic transitions there are phonon assisted interaction probabilities that give rise to the inter-band absorptions in the films corresponding to the energy levels in forbidden band. Excitons may be formed by direct photons only or by photon-phonon assistance. This direct absorption probability in the forbidden gap is given by Eq. (1) with $m = 3/2$; and the $\alpha^{2/3}$ *vs.* $h\nu$ plots are shown in Figs. 9(c), 10(c) and 11(c), for films prepared at different conditions. The values of direct forbidden gap energy (associated with this mechanism) were found to be 2.3, 2.06, and 2.12 eV, for the samples deposited at RT, at 300 °C substrate temperature, and for the samples annealed at 300 °C, respectively. Excitons may also be formed by photon-phonon interactions. The phonon assisted probabilities or indirect absorption probability in the forbidden gap is given by Eq. (1) with $m = 3$. Figs. 9(d), 10(d) and 11(d) shows $\alpha^{1/3}$ *vs.* $h\nu$ plot to obtain the indirect forbidden energy gap E_g, associated with this mechanism. The values of indirect forbidden energy gap E_g were found to be 2.24, 1.86, and 1.63 eV, for the samples deposited at RT, at 300 °C and for the samples annealed at 300 °C, respectively.

From these measurements, the most satisfactory representation is obtained for $\alpha^{1/3}$ *vs.* $h\nu$ plot, which suggests phonon assisted indirect forbidden transitions in the deposited $NaNbO_3$ films.

References

[1] Gunther P. Nonlinear optical crystals for optical frequency doubling with laser diodes. *Proc. SPIE*, 1981, **236**, P. 8–19.

[2] Okuyama M., Matsui Y., Nakano H., Hamakawa Y. $PbTiO_3$ ferroelectric thin film gate fet for infrared detection. *Ferrelectrctrics*, 1981, **33** (1), P. 235–241.

[3] Hewig G.H., Jain K. Frequency doubling in a $LiNbO_3$ thin film deposited on sapphire. *J. Appl. Phys.*, 1983, **54** (1), P. 57–61.

[4] Baumert J.C., Hoffnagle J., Gunther P. Nonlinear optical effects in $KNbO_3$ crystals at $Al_xGa_{1-x}As$, dye, ruby and Nd:YAG laser. *Proc. SPIE*, 1984, **492**, P. 374–386.

[5] Iijimo K., Tomita Y., Takayama R., Ueda I. Preparation of C-axis orientated $PbTiO_3$ thin films and their crystallographic, dielectric, and pyroelectric properties. *J. Appl. Phys.*, 1986, **60** (1), P. 361–367.

[6] Martin S.J., Butler M.A., Land C.E. Ferroelectric optical image comparator using PLZT thin films. *Electron. Lett.*, 1988, **24** (24), P. 1486–1487.

[7] Krishnakumar S., Oguz V.H., et al. Deposition and characterization of thin ferroelectric lead lanthanum zirconate titanate (PLZT) films on sapphire for spatial light modulators applications. *IEEE Trans. Ultrason. Ferrelec. Freq. Contr.*, 1991, **38** (6), P. 585–590.

[8] Ivey M., Mancha S., Carter R. Optical information storage and charge traps in PZT thin films. *IEEE Trans. Ultrson. Ferroelec. Freq. Contr.*, 1991, **38** (4), P. 337–343.

[9] Tamada H., Yamada A., Saitoh M. $LiNbO_3$ thin film optical waveguide grown by liquid phase epitaxy and its application to second-harmonic generation. *J. Appl. Phys.*, 1991, **70** (5), P. 2536–2541.

[10] Gutmann R., Hullinger J., Hauert R., Mosser E.M. Auger electron and x-ray photoelectrons spectroscopy of monocrystalline layers of $KTa_{1-x}Nb_xO_3$ grown by liquid-phase epitaxy. *J. Appl. Phys.*, 1991, **70** (5), P. 2648–2653.

[11] Polla D.I., Ye C., Tamagawa T. Surface-micromachined $PbTiO_3$ pyroelectric detectors. *Appl. Phys. Lett.*, 1991, **59** (1), P. 3539–3544.

[12] Sreenivas K., Mansingh A., Sayer M. Structural and electrical properties of rf-sputtered amorphous barium titanate thin films. *J. Appl. Phys.*, 1987, **62** (11), P. 4475–4481.

[13] Rabson T.A., Baumann R.C., Rost T.A. Thin film lithium niobate on silicon. *Ferroelectrics*, 1990, **112** (1), P. 265–271.

[14] Krupanidhi S.B., Mohan Rao G. Pulsed laser deposition of strontium titanate thin films for dynamic random access memory applications. *Thin Solid Films*, 1994, **249** (1), P. 100–108.

[15] Pignolet A., Mohan Rao G., Krupanidhi S.B. Rapid thermal processed thin films of reactively sputtered Ta_2O_5. *Thin Solid Films*, 1995, **258** (1–2), P. 230–235.

[16] Smith R.A. *Wave Mechanics of Crystalline Solids*. North Holland publication, Amsterdam, 1972.

[17] Rubio J.D., Albella J.M., Martinez-Duart J.M. Sputtered Ta_2O_5 antireflecting coating for silicon solar cells. *Thin Solid Films*, 1982, **90** (4), P. 405–408.

[18] Swanepoel S. Determination of the thickness and optical constants of amorphous silicon. *J. Phys. E: Sci. Inst.*, 1983, **16** (12), P. 1214–1222.

[19] Landolt H., Börnstein R. et al. *Numerical Data and Functional Relationships in Science and technology*, **16**, Group III, *Crystal and Solid State Physics*. Springer Verlag Berlin, Heidelberg-New York, 1981.

[20] Raevskii I.P., Reznichenko L. Phase transitions and electrical properties of ferroelectric solid solution based on $NaNbO_3$. *Izestiva Akademii Nauk SSSR, Neorganicheskie Mater.,* 1979, **15** (5), P. 872–875.

[21] Sze S.M. *Physics of Semiconductor Devices*. Wiley publication, New York, 2000.

[22] Pankove J.J. *Optical Processes in Semiconductors*. Prentice Hall, New Jersey, 1956.

[23] Sze S.M. Current transport and maximum dielectric strength of silicon nitride films. *J. Appl. Phys.*, 1967, **38** (7), P. 2951–2955.

[24] Kittel C. *Solid State Physics*. John Wiley and Sons, New York, 1970.

[25] Michael S. *Physics of Semiconductor Devices*. Prentice Hall of India Pvt. Ltd., New Delhi, 1995.